Hammett Parameter in Microporous Solids as Macroligands for Heterogenized Photocatalysts

F. Wisser, P. Berruyer, L. Cardenas, Y. Mohr, E. Quadrelli, A. Lesage, D. Farrusseng, J. Canivet

Hammett parameter in microporous solids as macroligands for heterogenized photocatalysts

Florian M. Wisser,[†,] Pierrick Berruyer,[‡] Luis Cardenas,[†] Yorck Mohr,[†] Elsje Alessandra Quadrelli,[Π] Anne Lesage,[‡] David Farrusseng,[†] Jérôme Canivet[†,]**

[†] Univ. Lyon, Université Claude Bernard Lyon 1, CNRS, IRCELYON - UMR 5256, 2 Avenue Albert Einstein, 69626 Villeurbanne Cedex, France. [‡] Univ. Lyon, Université Claude Bernard Lyon 1, Institut des Sciences Analytiques, ENS Lyon, CNRS, UMR 5280, 5 rue de la Doua, 69100 Villeurbanne, France. [Π] Univ. Lyon, Université Claude Bernard Lyon 1, CPE Lyon, CNRS, C2P2 - UMR 5265, 43 Bvd du 11 Novembre 1918, 69616 Villeurbanne, France..

ABSTRACT Here we present series of heterogeneous catalysts based on Metal-Organic Frameworks and Microporous Polymers used as macroligands for heterogenized organometallic complexes. We show that both homogeneous and heterogenized catalysts follow the same linear correlation between the electronic effect of the ligand, described by the Hammett parameter, and the catalytic activity. This correlation highlights the crucial impact of the local electronic environment surrounding the active catalytic center over the long-range framework structure of the porous support. The rational design of heterogenized catalysts can thus be guided by molecular chemistry rules. The conception of highly efficient heterogeneous catalyst based on porous

polymer support and driven by the Hammett parameter of bipyridine-chelating macroligand is demonstrated here for the Rh-catalyzed photoreduction of carbon dioxide with turnover frequencies up to 28 h^{-1}, among the highest reported for heterogeneous photocatalytic formate production.

KEYWORDS conjugated microporous polymers; microporous materials; photocatalysis; carbon dioxide reduction; rhodium complex; Hammett constant.

1. Introduction

The understanding of the mechanisms driving heterogeneously catalyzed reactions is a challenge continuously addressed. The heterogenization of well-defined catalytically active species onto a solid support is an appealing approach to get insight into catalyst behavior at the molecular level.[1-3]

In addition to the easy separation from the products and to recyclability,[4-8] grafting active catalysts onto a surface allows isolating catalytically active centers from each other, minimizing interaction between them, preventing possible multi-metallic decomposition and thus favoring the maintenance of optimal catalytic activity.[9] To enhance the mass loading of heterogenized catalysts, meso- and microporous materials have been investigated as supports with high surface-area-to-volume ratios.[9-10] Nonetheless, the integration of the catalytically active centers into a solid support without loss of performance compared to the homogeneous analog remains a major challenge.[4, 8-9, 11-12]

In this context, a molecularly defined support as macroligand,[13] *i.e.* a larger molecule or a solid acting like the ligand in the corresponding molecular complex, can be considered as a key to bridge the gap between molecular and heterogeneous catalysis. Hybrid organic-inorganic Metal-

Organic Frameworks (MOF) [14-18] and purely organic porous polymers,[19-22] such as conjugated microporous polymers (CMP),[23-26] are promising candidates. In particular, porous frameworks based on the bipyridine (Bpy) motif are of a high interest as far as Bpy sites are widely used as chelating ligand for molecular catalysts.[27]

Here, we show that the Hammett parameter – well established in molecular chemistry and homogeneous catalysis[28-31] – is also an appropriate descriptor for heterogenized organometallic catalytic centers. This has been made possible thanks to the use of macroligands as solid hosts, which are Bpy-containing MOF, namely UiO-67[32] and MOF-253,[33] and CMP-related materials including four newly synthesized porous polymers. We demonstrate that this rule from molecular chemistry can be applied to the design of heterogeneous catalysts.

2. Results and discussion

2.1. Hammett parameter-driven design of porous hosts

In molecular chemistry, the electronic effects of the substituents are typically described using the Hammett constant (σ), which allows the direct comparison of the molecular-level influence of different functional groups on the reaction rate.

The theory shows that the substituent's electronic effects are additive and therefore give a large latitude in tunability.[30] Thus we synthesized a series of Cp*Rh(bpy)-containing MOF and functionalized CMP materials (**Scheme 1**), in order to explore a large range of Hammett constants and study the influence on the heterogeneous rhodium-based catalytic activity.

Scheme 1. Library of different *meta* substituted 2,2'-bipyridine ligands embedded in MOF or CMP materials studied herein (σ_m = Hammett constant of substituent).

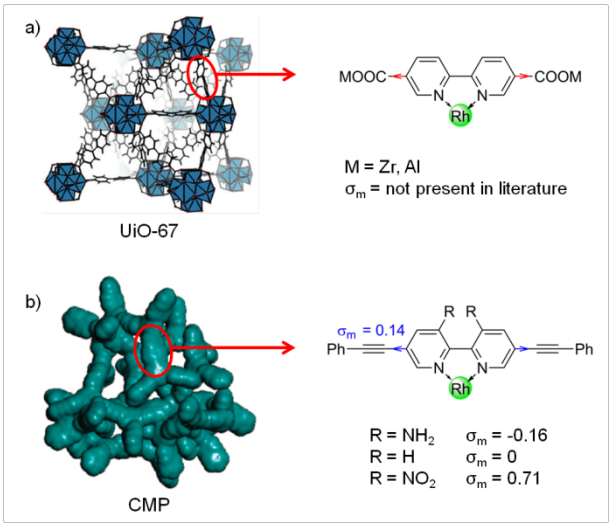

Representative structures of Cp*Rh(bpy) species embedded in (a) MOF[34] and (b) CMP.[35] Rh stands for $[Cp^*RhCl]^+$ moiety used as catalytic active center. Structures reproduced with permission from ref. 34 and 35. Copyright 2016 John Wiley and Sons and 2008 American Chemical Society.

2.1.1. Synthesis of new Bpy-based porous polymers

We prepared four new bipyridine-containing microporous polymers (BpyMP) based on CMP structures which were then post-synthetically modified with a rhodium complex (**Scheme 2**). The two BpyMP series prepared differ in their respective connecting subunit. A phenyl ring ensures the electron conjugation in BpyMP-1 while a non-conjugating tetrakismethane is used in BpyMP-2. We synthesized the BpyMP platforms by copolymerization of polyethynyl tectons with a stoichiometric amounts of a mixture of 5,5'-dibromo-2,2'-bipyridine derivatives (25 mol-% of the stoichiometric amount) and 4,4'-diiodo-biphenyl (75 mol-%) (**Scheme 2**, see SI for experimental details).[36] As polyethynyl tecton, 1,3,5-triethynylbenzene has been used for the BpyMP-1 series and tetrakis(ethynyl-phenyl)methane for the BpyMP-2. Considering Bpy-based monomers, 5,5'-dibromo-2,2'-bipyridine has been used for BpyMP-1 and BpyMP-2, 5,5'-

dibromo-3,3-diamino-2,2'-bipyridine for BpyMP-1-NH_2 and 5,5'-dibromo-3,3-dinitro-2,2'-bipyridine for BpyMP-1-NO_2. In contrast to known bipyridine containing CMP's,[37-39] the co-monomers 5,5'-dibromo-2,2'-bipyridine and 4,4'-diiodo-biphenyl have the same length to give a more regular polymer and we followed the stochiometric approach introduced recently by the Thomas group which avoids unwanted side reactions such as homocoupling and give rise to materials with higher porosity.[36] The BpyMP frameworks were obtained as yellow to dark orange powders consisting of aggregated spherical particles with diameters below 1 µm (**Figure S5** & **Figure S6**).

The rhodium-functionalized catalysts were prepared by infiltration of the material in a methanol solution of [RhCp*Cl]NO_3 for 24 h (Scheme 2, for details see SI). For BpyMP-1, various Rh loadings (ω_{Rh}), *viz.* between 0 and 4.0 wt% (named hereafter *x*%Cp*Rh @ BpyMP-1, **Table S1**) were prepared. For Bpy-MP-1-NH_2 and BpyMP-2, samples with a Rh loading of 1.6 wt% and for BpyMP-1-NO_2 with 1.0 wt% Rh were synthesized (**Table S1**). The Rh contents of all samples, determined by ICP-OES, are in line with the nominal content, confirming the complete incorporation of Rh into the polymer, except for the highest loading (4.0 wt% instead of 4.5 wt% nominal loading).

Scheme 2. Preparation of microporous polymers as host for Cp*Rh-catalysts.

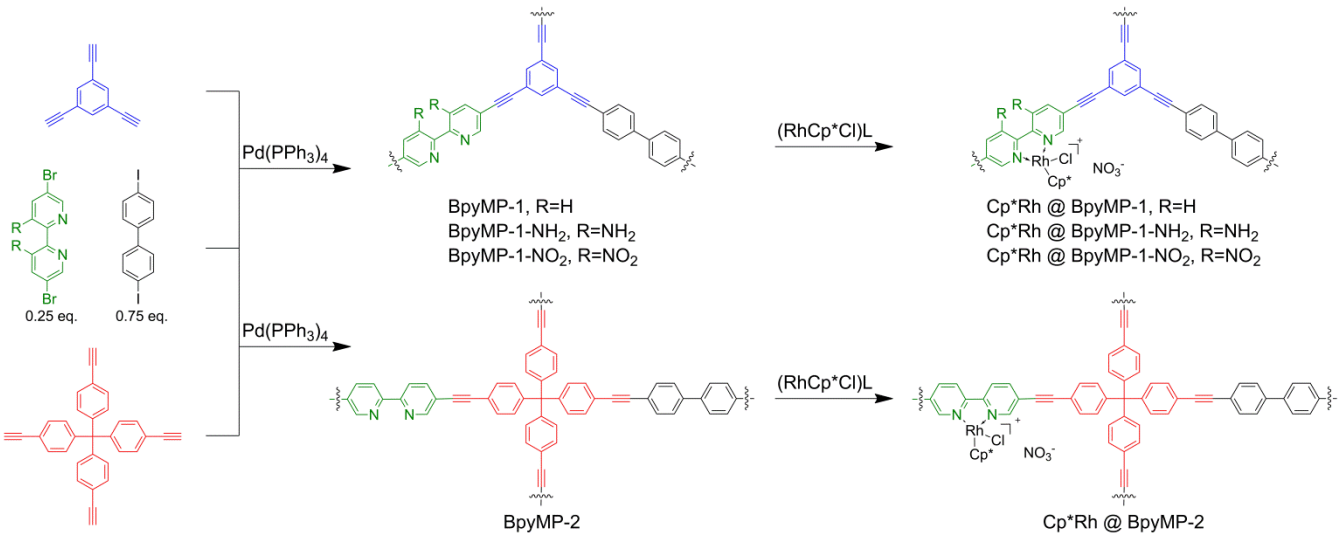

BpyMP-1, BpyMP-1-NH_2 and BpyMP-1-NO_2: based on 1,3,5-triethynylbenzene containing 25 mol-% of bipyridine monomers. BpyMP-2: based on tetrakis(ethynylphenyl)methane containing 25 mol-% of bipyridine monomers.

2.1.2. Spectroscopic characterizations

In order to reach enough sensitivity, the molecular structure of the porous polymers was investigated by Dynamic Nuclear Polarization (DNP) Surface Enhanced NMR Spectroscopy (SENS).[40-42]

Two new signals at 94.3 ppm and 8 ppm are observed in the 1D ^{13}C CP MAS spectra of all polymer base catalysts after rhodium addition. These signals can be assigned to quaternary carbon atoms and to methyl groups of the pentamethyl-cyclopentadienyl (Cp*) moiety of the metal complex (**Figure S10**, **Figure S11**). The 2D HETCOR spectrum shows the expected correlations for the resonances of the Cp* ligands (**Figure S13**).[36]

In UV-Vis spectra, both the absorption maximum and the band gap are gradually shifted to lower energies with increasing the Rh content in the polymeric materials (**Figure S15**). The optical band gap is reduced from 2.65 eV for BpyMP-1 to 2.52 eV for 4.0%Cp*Rh @ BpyMP-1. For the BpyMP-2 based catalyst the same red shift of ~0.1 eV is observed (2.65 to 2.55 eV, 1.6 wt%

Rh). The amine functionalized polymer BpyMP-1-NH_2 has a smaller band gap of 2.31 eV, which is also red-shifted by ~0.17 eV to 2.14 eV after infiltration with the rhodium precursor (1.6 wt% Rh). In case of BpyMP-1-NO_2 a blue shift of about 0.05 eV to 1.99 eV is observed after Cp*Rh infiltration. Such influence of the framework substitution on the optical band gap, linked to their photocatalytic activity, has also been reported for MOF materials.[43-44] In each case, the gap shifts prove the coordinative fixation of the Rh center on the polymer framework.

2.1.3. Porosity measurement

All BpyMP-based materials show a permanent porosity in nitrogen physisorption experiments at 77 K (**Figure 1a** and **Figure S22**). The isotherms show the characteristic swelling behavior of microporous polymers, indicated by a difference between the adsorption and desorption branches of the isotherm over the entire pressure range (hysteresis, **Figure 1a**).[45] Even if the quantitative analysis of isotherms for swelling materials might be questionable because the density is not corrected during the measurement (for further discussion see SI), we can show that all supports obtained are mostly microporous (**Figure 1a**).

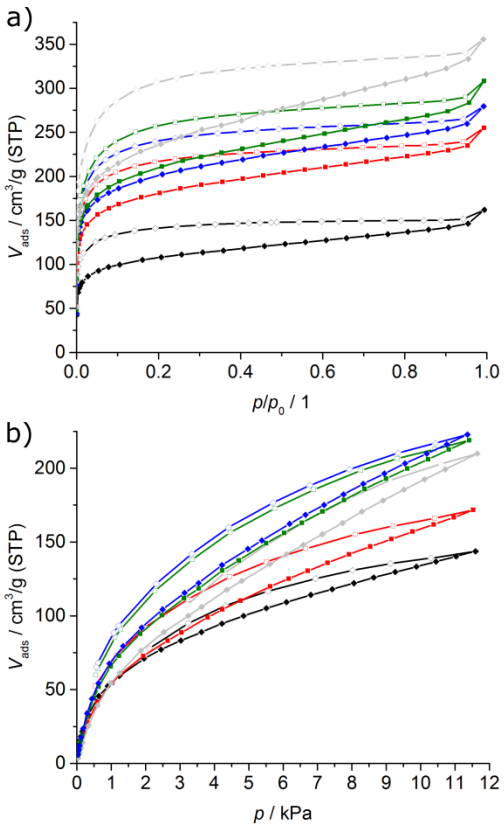

Figure 1. a) N_2 physisorption isotherms measured at 77 K and b) acetonitrile vapor physisorption isotherms measured at 298 K of BpyMP-1 (pale grey), 1.0%Cp*Rh @ BpyMP-1 (green), 1.6%Cp*Rh @ BpyMP-1 (blue), 2.4%Cp*Rh @ BpyMP-1 (red) and 4.0%Cp*Rh @ BpyMP-1 (black).

Upon Rh incorporation, the apparent surface area decreases from approximately 680 ± 30 m^2/g for BpyMP-1 to nearly half the initial value for 4.0%Cp*Rh @ BpyMP-1 (280 ± 60 m^2/g). The accessible pore volume decreases continuously with Rh content from 0.45 ± 0.04 for BpyMP-1 to 0.21 ± 0.02 cm^3/g for 4.0%Cp*Rh @ BpyMP-1 (**Table S2**). The same trend is observed for BpyMP-1-NH_2 and 1.6%Cp*Rh @ BpyMP-1-NH_2, BpyMP-1-NO_2 and 1.0%Cp*Rh @ BpyMP-1-NO_2 as well as Bpy-MP-2 and 1.6%Cp*Rh @ BpyMP-2 (**Figure S22**). The reduced pore

volumes upon metalation can suggest pore blocking by the catalyst, which may decrease the number of accessible catalytic sites (*vide infra*).

For a better understanding of solvent interaction processes under conditions relevant to the real catalysis situation, acetonitrile vapor isotherms were recorded at 298 K for all materials (**Figure 1b**, **Figure S25** & **Table S2**).

The total volume of acetonitrile vapor adsorbed remains constant up to 1.6 wt% of rhodium, indicating that no or only negligible pore-blocking occurs. For higher loadings, the decrease in total pore volume indicates non-negligible pore blocking (*vide infra*). Moreover, the smaller differences between the adsorption and desorption branches of the acetonitrile physisorption isotherms with increasing Rh content can be attributed to a reduced swelling behavior, resulting in reduced flexibility and, as a consequence, lower accessibility of the network.[46-47]

In the light of the work published by Cooper and coworkers on CMP materials,[24] one would expect the porous system in our BpyMP solids to be three dimensional, with estimated pore sizes for the micropores between 0.6 and 1.6 nm, independent of the functionalization of the framework and its monomers composition. We note that only rough estimations of the pore size distributions can be given, as the materials are flexible (further discussion are given in the SI).[20, 48]

2.2. Catalytic activity

2.2.1. CO_2 photoreduction

In order to assess the correlation between the catalytic activities of the MOFs and BpyMP-based materials and the Hammett parameters, we used the CO_2 photoreduction as model catalytic reaction.

Formic acid and formate-amine mixtures are currently being discussed as hydrogen storage molecules for fuel cell applications as these products have a relatively high volumetric hydrogen content. They can be stored and handled easily and at the same time are catalytically decomposable at low temperatures.[49-53] Depending on the conditions, different value-added C1 molecules such as formic acid, methanol or methane are produced by CO_2 photoreduction.[54-57] Catalytically active centers can be grafted onto the MOF linkers containing chelating groups such as catechols or bipyridines have been already reported using Mn, Ir, Re or Rh for photochemical CO_2 reduction.[58-63] Turnover frequencies (TOF) of up to 16 h^{-1} for formate have been achieved under typical conditions,[63] e.g., triethanolamine as reductant in acetonitrile or dimethylformamide as solvent.[54]

As in MOFs, the synthesis of microporous polymers allows for the incorporation of bipyridine-based organo- and photocatalysts, especially for photochemical hydrogen evolution and hydrogenation of CO_2.[8, 64-68] Only Liang *et al.* have reported a porous polymer as host material for photocatalytic CO_2 reduction based on (α-diimine)$Re(CO)_3Cl$ moieties into a bipyridine-functionalized CMP-5 network. Using this catalyst they obtained a mixture of CO and H_2.[38]

2.2.2. Activity of BpyMP and related MOF materials

Based on the reported activity of molecular and MOF-heterogenized Cp*Rh(bpy) complexes in carbon dioxide photoreduction,[59] we evaluated the catalytic performances of our four Cp*Rh@BpyMP solids and two Cp*Rh@MOF representatives.

Catalytic tests were conducted in acetonitrile-triethanolamine (ACN:TEOA, 5:1, *V*:*V*) solution containing 1 mM of $Ru(bpy)_3Cl_2$ as photosensitizer.[59] The production rate being constant for the first four hours of reaction, the TOF were determined from the formate production after four hours of reaction (**Figure S35**). As previously shown for Cp*Rh(bpy)@UiO-67,[59] selective reduction of CO_2 to formate without any other carbon-containing byproduct is observed for all the materials.

For Rh@BpyMP-1 containing 0.7 to 1.6wt% of rhodium, the TOF increased to reach a plateau at ca. 24.5 ± 0.5 h^{-1} for ω_{Rh} = 1.3 to 1.6 wt% then decreased drastically for higher loadings (**Figure 2**, **Table S3**). This suggests that the accessibility of the Rh catalyst inside the pores might be reduced for high loadings due to pore blocking and reduced flexibility, as observed in N_2 and acetonitrile vapor physisorption measurements.[69] The product evolution rate *R*, expressed in $mmol_{(formate)} \cdot h^{-1} \cdot g_{(catalyst)}^{-1}$,[57] increased linearly up to ω_{Rh} = 1.6 wt% and remained constant for higher loadings (**Figure 2**). The optimal loading for the BpyMP-1 network is thus around ω_{Rh} = 1.6 wt% with *R* = 3.7 ± 0.1 $mmol \cdot h^{-1} \cdot g_{cat}^{-1}$ and TOF = 24.2 ± 0.5 h^{-1}, giving a well-balanced equilibrium among the number of active centers, the remaining porosity and thus the accessibility of the active centers and the catalytic performance.

It is worth noting that formation of formate over pristine BpyMP-1 (see Table S3, ω_{Rh} = 0 wt%, *R* = 0.18 ± 0.1 $mmol/h/g_{cat}$) occurs and is most likely caused by the photolabilization of one bipyridine ligand in the $[Ru(bpy)_3]Cl_2$ photosensitizer, yielding a catalytically active ruthenium(II)-bis-bipyridine complex (see **Table S3**, 1.63 μmol of formate produced using only

$Ru(bpy)_3Cl_2$ without catalyst) as shown by Lehn *et al.*.[70-71] This effect is however not significant compared to the twenty times higher product evolution rate obtained using 1.6%Cp*Rh @ BpyMP-1 catalyst. Similarly, the low formate production using the pristine BpyMP-material without rhodium as catalyst shows that the impact of the palladium species (~0.5 wt%, **Table S1**) remaining from the BpyMP synthesis is also negligible.

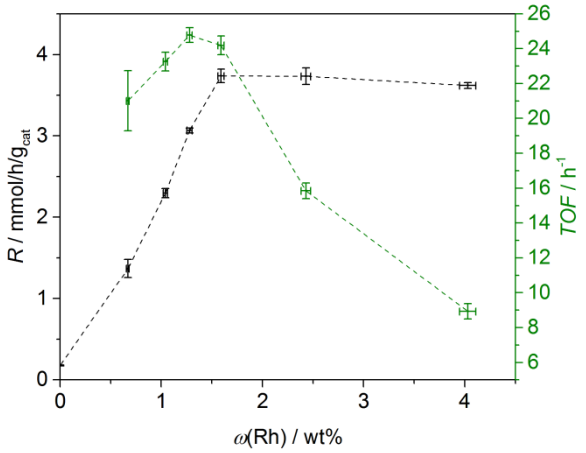

Figure 2. Product evolution rate *R* (black) and TOF (green) as a function of rhodium mass fraction in the porous polymer BpyMP-1.

Formate decomposition experiments using ^{13}C-formate in argon-saturated ACN/TEOA show that in the BpyMP system no substantial formate decomposition into CO_2 / HCO_3^- and H_2 occurs (see SI for experimental details, Figure S37 & Figure S38). The rate of formate decomposition using 4.0%Cp*Rh @ BpyMP-1 (0.20 µmol/h/g_{cat}) is reduced by three orders of magnitude compared to the rate obtained when using rhodium-functionalized UiO-67 (0.25 mmol/h/g_{cat} with ω_{Rh} = 7.4 wt%).[59] Compared to the rate of catalysis (up to 3.7 mmol/h/g_{cat}), the formate decomposition has a negligible impact. Suppressing back reaction is of vital importance for the development of heterogeneous molecular catalysts.[8]

The stability of the BpyMP materials was proven by IR spectroscopy and nitrogen sorption after recycle experiments and heterogeneity tests with 1.6%Cp*Rh @ BpyMP-1 (**Figure S40**). Over

five cycles of catalysis using the same catalyst, the TOF remains constant at 23.1 ± 0.6 h^{-1} (**Figure S39a**). In addition, leaching tests were carried out by removing the catalyst, saturating the solution with CO_2 and irradiating the solution for another 2 or 4 hours (**Figure S39b**). No change in the amount of formate being detectable, we thus excluded the leaching of active centers from the material into the solution.

The 1.6%Cp*Rh @ BpyMP-1 catalyst has also been exposed to direct sunlight and showed a TOF of 3.69 ± 0.27 h^{-1} using the same ACN-TEOA-$Ru(bpy)_3Cl_2$ solution (**Table S3**, **Figure S36**). It has to be noted that the sun's irradiation used here is weaker by a factor of at least 2 with respect to solar simulators, without taking into account the time-dependent change of the angle of incidence of the light on the glass reactor (see SI for detailed information).

The highest product evolution rate being achieved for BpyMP-1 with ω_{Rh} = 1.6 wt%, we investigated the catalytic potential of BpyMP-2, BpyMP-1-NH_2 and BpyMP-1-NO_2 platforms with this optimal Rh loading. The evaluation of the polymeric network BpyMP-2, which is based on non-conjugated tetrakis(4-ethynylphenyl)methane instead of 1,3,5-triethynylbenzene found in BpyMP-1 (**Figure 3**), gives identical TOF and *R* value with 22.5 ± 1.4 h^{-1} and 3.6 ± 0.2 mmol/h/g_{cat}, respectively, for ω_{Rh} = 1.6 wt% (**Figure 3**). This result reveals that the overall structure of the polymer host material, e.g., the size of the conjugated π-system and pore size, has a negligible impact on the catalytic activity for optimized Rh loadings.

BpyMP-1-NO_2 having nitro electron-withdrawing groups shows the lowest activity with a TOF = 2.40 ± 0.57 h^{-1}. BpyMP-1-NH_2, with two NH_2 electron-donating groups, shows the highest TOF value of 28.3 ± 1.6 h^{-1} (**Figure 3**).

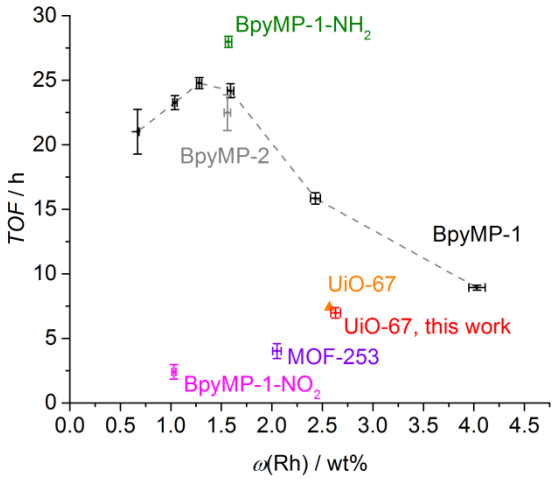

Figure 3. TOF for BpyMP-1 (black), BpyMP-1-NH_2 (green), BpyMP-1-NO_2 (pink), BpyMP-2 (gray), UiO-67 (red) and MOF-253 (purple) based catalyst as a function of the Rh loading. The value for UiO-67 (triangle, orange) was taken from Ref. [59].

These data highlight the crucial impact of the local electronic environment surrounding the active catalytic center over the long-range framework structure.

The Cp*Rh@UiO-67 with an optimized molar Rh loading of 10 mol-%, corresponding to ω_{Rh} = 2.6 wt% has been prepared following our previously published procedure.[59] Using this catalyst in our present setup, an *R* value up to 1.8 ± 0.1 mmol/h/g_{cat} corresponding to a TOF = 7.0 ± 0.4 h^{-1} was achieved (**Figure 3**, **Table S3**).

The 2.1%Cp*Rh@MOF-253 has been prepared and characterized following a procedure similar to that applied to UiO-67 (see SI for synthesis and characterizations details). Under the same conditions, this catalyst shows a TOF value of 4.01 ± 0.58 h^{-1}. We attribute the difference in activity between the two MOF studied by the stronger electron withdrawing effect of aluminum-carboxylate in MOF-253 compared to zirconium-carboxylate in UiO-67. We will rationalize and quantify this difference on the basis of the Hammett parameter in the next section.

Finally we ensure that the wettability of the host material does not influence the catalytic activity as far as the interaction with the acetonitrile solvent is very similar for MOF and all BpyMP materials (see the Henry constant K_H in the **Table S1**).[72]

To the best of our knowledge, we present here the highest TON (up to 113) and TOF values (up to 28 h^{-1}) for CO_2 reduction to formate achieved with a heterogenized catalyst within a porous polymer, through the use of 1.6%Cp*Rh @ BpyMP-1-NH_2. Product evolution rates are enhanced by at least one order of magnitude with respect to comparable systems known in the literature (see **Table S4** & **Table S5**).[57]

2.3. Quantification of the structure-activity relationship

2.3.1. Determination of the σ value of the supports

In purely organic microporous polymers, that are prepared by coupling terminal alkynes with aromatic halides,[24] the Hammett constant can be set to σ_m = 0.14 using the literature value of a phenylethynyl substituent at the *meta* position as found in BpyMP-1 and BpyMP-2 (**Scheme 1b**).[30] The presence of an additional amino group at the second *meta* position of the pyridine moiety (on C^3 and $C^{3'}$) with a Hammett constant of -0.16 [29-30] confers to the N atom a further increased electron density, with an averaged σ_m = -0.02 for BpyMP-1-NH_2.

In MOF hybrid solids, the determination of the Hammett parameter is less trivial. Kitagawa and co-workers mentioned Hammett parameter when observing that the CO stretching vibration of a Ru-CO-complex grafted into UiO-67 becomes stronger than that of the molecular analog coordinated by the 2,2'-bipyridine-5,5'-dicarboxylic acid.[63] De Vos, Van Speybroeck and co-workers have reported a phenomenological correlation between the relative rate constants of Zr-based Lewis acid catalysis by isostructural UiO-66 MOF and the Hammett constant.[73-74] Since

only isostructural MOFs were compared to each other, no electronic effect of the metal-oxide node was taken into account nor quantified.

Thus we determined the σ_m value of metal-carboxylate at the *meta* position of a pyridine in UiO-67 and MOF-253.

We used the linear correlation between CO vibration wavenumber and corresponding Hammett constant[75-76] established for molecular and BpyMP-supported Re(CO) and Ru(CO) complexes (see SI)[62, 77-78] to determine that zirconium-carboxylate in UiO-67 shows a σ_m = 0.48 and aluminum-carboxylate in MOF-253 a σ_m = 0.66 (**Figures S2** and **Figure S3**). This large difference highlights the strong influence of the inorganic node nature on the electron density on the MOF linker.

2.3.2. Correlation σ vs TOF in both homogeneous and heterogeneous systems

The correlation between catalytic activity and Hammett constant has already been demonstrated for molecular homogeneous complexes[31, 79] but neither for photocatalytic CO_2 reduction nor for catalytic systems including both homogeneous and heterogeneous representatives.

We observed that the measured activities for the three molecular Cp*Rh catalysts **1 – 3** (**Scheme 3**) with well established σ_m values follow a linear correlation between σ_m and log(TOF) in CO_2 photoreduction Figure 4 and Table 1, entries 2, 5 and 6).

Scheme 3. Cp*Rh(bipy) molecular complexes used for establishing linear correlation between TOF and σ_m

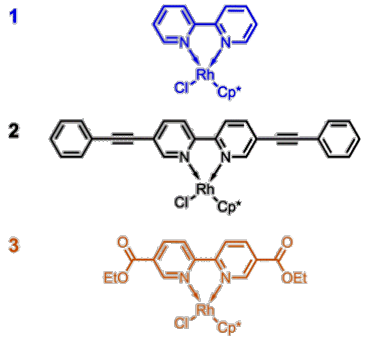

Cp*Rh(2,2'-bipyridine)Cl_2 (**1**) used as electronically-neutral reference, Cp*Rh(5,5'-bis(phenyl-ethinylene)-2,2'-bipyridine)Cl_2 (**2**) as molecular analogue to BpyMP-1 and Cp*Rh(diethyl(2,2'-bipyridine)-5,5'-dicarboxylate)Cl_2 (**3**) as molecular analogue Cp*Rh@UiO-67 / Cp*Rh@MOF-253 catalysts.

The lg(TOF) values for Cp*Rh-functionalized BpyMP-1, BpyMP-1-NO_2, BpyMP-2 as well as UiO-67 and MOF-253 using the σ_m values of the solids follow exactly the same fit (**Figure 4**). According to the data obtained for Cp*Rh @ BpyMP-1-NH_2, the TOF measured deviates from the linear trend (**Figure 4a**). In order to assess the origin of the deviation, *i.e.* diffusion limitation or lower intrinsic activity, we investigated the activity of amino-functionalized molecular complex **4** (**Figure 4a**, Inset). Under the same conditions, both Cp*Rh @ BpyMP-1-NH_2 and **4** show a TOF lower than the one expected according to their calculated σ_m value (**Table 1**, entries 1 and 7). Since **4** is in homogeneous condition, such lower activities cannot be attributed to diffusion limitation.

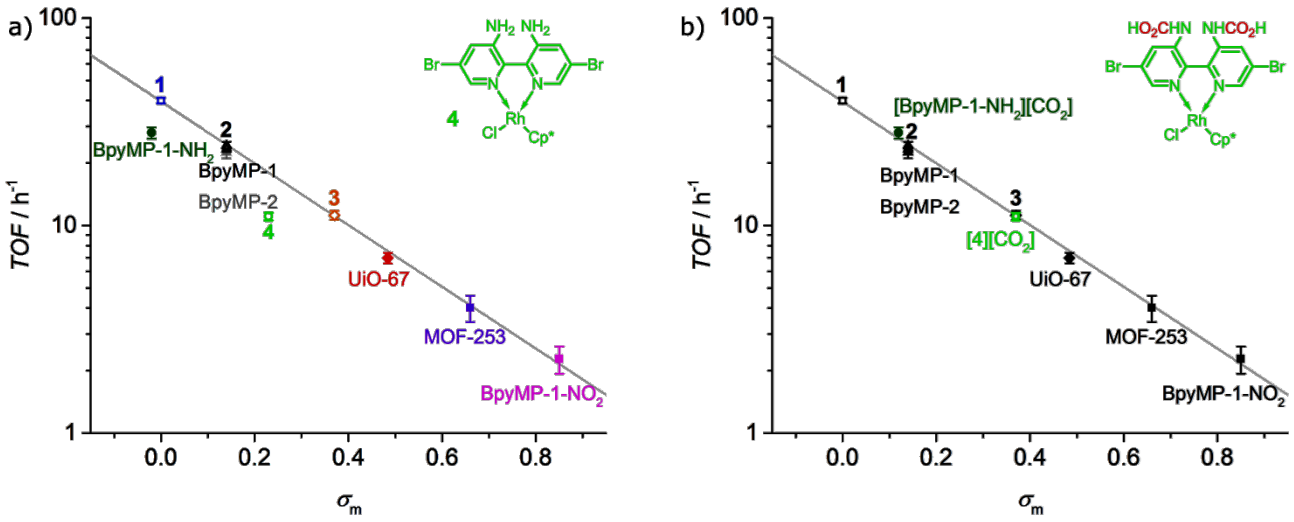

Figure 4. Hammett plots of log(TOF) as a function of the Hammett constant σ_m of the Bpy ligand. Open and close symbols correspond to homogeneous and heterogeneous catalysts, respectively. The Hammett constant used is (**a**) σ_m = - 0.16 for NH_2 groups in BpyMP-1-NH_2 and **4** or (**b**) σ_m = - 0.02 for NHCOOH groups in the corresponding CO_2 adducts. The insets show (**a**) the molecular structure of complex **4** and (**b**) the idealized CO_2 adduct of **4** as carbamic acid.

The established linear fit shown on the **Figure 4** allows determining, from the corresponding TOF, Hammett parameter values σ_m = 0.12 instead of -0.02 for BpyMP-1-NH_2 and σ_m = 0.37 instead of 0.23 for **4** (**Table S3**). These estimated σ_m values are both +0.14 higher than the one calculated using the contribution of amino NH_2 groups (**Table 1**, entries 1 and 7). These corrected σ_m values can correspond to the contribution of carbamic acid NHCOOH groups formed *in situ* by the interaction of carbon dioxide with amino groups. Indeed such $[NH_2][CO_2]$ interaction giving carbamate species has already been described in aniline/acetonitrile solutions and in MOF for CO_2 adsorption using DFT calculations.[80-81] Our hypothesis is further supported by the observation of carbamate derivative of 3,3'-diamino-5,5'dibromo-2,2'-bipyridine (ligand of

complex **4**) under catalytic conditions in deuterated solution using NMR spectroscopy (see **Figure S42**).

Table 1. Overview over the different ligands used, their corresponding Hammett constant (σ_m) and the average TOF of the optimized Cp*Rh-based catalysts.

#	Nature of the catalyst	ligand	σ_m	TOF / h-1
1	Heterogeneous	BpyMP-1-NH_2	-0.02	27.98 ± 1.74
2	Homogeneous	1	0	39.96 ± 1.21
3	Heterogeneous	BpyMP-1	0.14	23.46 ± 0.69
4	Heterogeneous	BpyMP-2	0.14	22.49 ± 1.39
5	Homogeneous	2	0.14	24.21 ± 1.13
6	Homogeneous	3	0.37	11.22 ± 0.55
7	Homogeneous	4	0.23	11.06 ± 0.47
8	Heterogeneous	UiO-67	0.48	6.97 ± 0.41
9	Heterogeneous	MOF-253	0.66	4.01 ± 0.58
10	Heterogeneous	BpyMP-1-NO_2	0.85	2.28 ± 0.34

Methyl carbamate shows a σ_m = -0.02 which is +0.14 higher than the σ_m = -0.16 of amino groups. The presence of carbamate groups, replacing the original amino, would confer to the [BpyMP-1-NH_2][CO_2] adduct an averaged σ_m = 0.12 and to the [**4**][CO_2] adduct a σ_m = -0.02 (**Figure 4b**, Inset). In this case, the activity measured for the two amino-functionalized catalysts are aligned with those of the other homogeneous and heterogeneous catalysts (**Figure 4b**). The catalytic activity of Cp*Rh @ BpyMP-1-NH_2 is thus not limited by diffusion inside the porous

system but by the unexpected *in situ* interactions with the carbon dioxide reactant leading to a change in electron density on the Rh active site.

The perfect correlation between the four homogeneous and the six heterogeneous systems studied shows that no diffusion limitation occurs in the porous materials under the investigated reaction conditions.

2.3.3. Correlation σ vs electron density in heterogeneous catalysts

In molecular chemistry, a low Hammett constant indicates a strong electron-donating effect of the substituent[28-31] and higher activity is often linked to higher electron density on the active site.[31] The perfect fit of the values from heterogeneous BpyMP-1, BpyMP-1-NO_2, BpyMP-1-NH_2, BpyMP-2, UiO-67 and MOF-253 catalysts with values from molecular catalysts suggests that the electronic structure of these heterogenized species is the same than that of their homogeneous analogues.

In order to quantify the electronic effect of the microporous macroligand on the heterogenized active rhodium center, we performed XPS analysis on the Rh3d core level.

In the XPS spectra, the contribution is located at 309.3 eV ($Rh^{III}3d_{5/2}$) in the BpyMP-1 based catalysts, at 309.3 eV in the BpyMP-2 based catalyst and at 309.1 eV in the BpyMP-1-NH_2 based catalyst, respectively (**Figure 5a**). The binding energies increase to 309.6 eV for Cp*Rh heterogenized in UiO-67 and to 309.8 eV for Cp*Rh heterogenized in MOF-253, independently of the loading and counterion (**Figure S17** & **Figure S20**). The value for BpyMP-1-NO_2 cannot be accurately determined as the sample shows strong electrostatic charging during XPS investigation (see also **Figure S19**). The linear fit obtained for the correlation between Rh binding energy and σ parameter of the corresponding macroligand evidences the dependence of

the electron density on the rhodium center to the electronic effect of the solid support (**Figure 5b**, **Figure S4**) and proves that rules from molecular chemistry can be accurately applied to solid porous macroligands like MOF and Microporous Polymers.

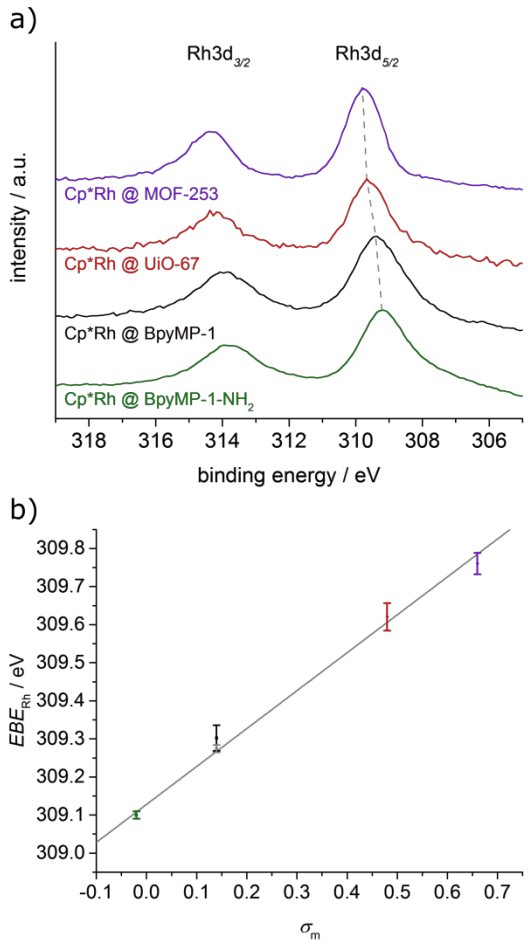

Figure 5. a) Rh3d XPS spectra of Cp*Rh @ BpyMP-1-NH_2 (green), Cp*Rh @ BpyMP-1 (black), Cp*Rh @ BpyMP-2 (gray), Cp*Rh@UiO-67 (red) and Cp*Rh@MOF-253 (purple). b) Linear correlation between the Rh binding energy and the Hammett parameter σ calculated in the solid macroligands (R^2 = 0.995).

3. Conclusion

Using carbon dioxide photoreduction as model catalytic reaction, we have shown here that the Hammett parameter is a common descriptor of the active site structure, directly linked to the catalytic activity, for both homogeneous and heterogeneous organometallic catalysts. It has been demonstrated for bipyridine systems in four molecular complexes, two MOF-based and four Microporous Polymers-based catalysts. The established correlation between the catalytic activity and the Hammett parameter highlights the crucial impact of the local electronic environment surrounding the active catalytic center over the long-range framework structure. The general linear trend gives also insight into the contribution of the diffusion limitation inside the porous network of such heterogeneous catalysts or of unexpected reactivity of functional groups at the macroligand.

With an optimal Rh loading of 1.6wt%, the newly-synthesized organic porous polymers BpyMP-1-NH_2 shows a photocatalytic CO_2-to-formate product evolution rate as high as 4.2 ± 0.1 mmol/h/g_{cat}. The corresponding TONs (up to 113) and TOFs (up to 28 h^{-1}) are the highest reported so far for heterogenized photocatalysts.

Both MOF and Microporous Polymers thus appear as very appealing platforms and their use as macroligands for the heterogenization of molecular catalysts is further reducing the gap between homogeneous and heterogeneous catalysis.

4. Experimental Section

Polymerization

The synthesis of BpyMP materials was done according to a modified literature procedure.[36]

For a typical synthesis of BpyMP-1, 50.0 mg (0.33 mmol) 1,3,5-triethynylbenzene, 155.4 mg (0.38 mmol) 4,4'-diiodobiphenyl, 39.8 mg (0.12 mmol) 5,5'-dibromo-2,2'-bipyridine and 7.5 mg (6.4 µmol) $Pd(PPh_3)_4$ were added to a flame dried Schlenk tube inside a glove box. The Schlenk tube was sealed with a teflon septum. Outside the glove box, 6 ml of anhydrous DMF and 3 ml of anhydrous NEt_3 were added and the glass vial was placed in an oil bath. The reaction mixture was heated to 100 °C for 24 h. After cooling down to room temperature, the polymer was precipitated by adding MeOH. The yellow solid was removed by centrifugation, suspended in 10 ml MeOH and removed by centrifugation after 1 h. The solid was additionally purified by soxhlet extraction using $CHCl_3$ for 6 h and using MeOH overnight. The yellow solid was dried at 80°C under vacuum. Typical yield: 110 mg.

Functionalization of BpyMP-networks

In a glass vial, 28.0 mg (44.9 µmol, 89.7 µmol $[Cp^*RhCl]^+$) $[Cp^*RhCl_2]_2$ and 15.2 mg (89.4 µmol) $AgNO_3$ were dispersed in a mixture of 5 ml anhydrous acetonitrile and 1 ml anhydrous MeOH and stirred for 2 h under light exclusion. The white solid was removed by centrifugation and the yellow solution was stored at 5°C.

For a typical infiltration, (10 mol-% Rh) 80 mg BpyMP-1 were dispersed in 3.7 ml dry MeOH, then 1.34 ml of the above-mentioned solution were added and the suspension was stirred for 24 h at room temperature. The supernatant was removed by centrifugation and the solid washed with MeOH during 2 days (exchange of MeOH every 12 h). The solid was dried under reduced pressure first at room temperature, then at 80°C.

Catalysis

For a typical catalysis, about 1 mg of the porous framework was weighed into an UV-VIS cuvette (path length: 10 mm). Then 2.2 ml of 1 mM $Ru(bpy)_3Cl_2$ in a mixture of acetonitrile and triethanolamine (5 : 1, *V* : *V*) were added and the solution was saturated with CO_2 for 15 min. The cuvette was sealed and the solution was irradiated for 4 h using a 200 W Hg(Xe) lamp (Newport Research Arc Lamp), equipped with a 420 nm UV cut-off filter and a water based IR filter unit, cut-off 950 nm, using a working distance 10 cm, and an irradiance of 1030 W/m^2. After 4 h the solvent was removed by centrifugation and the liquid phase was analyzed by *q*-^{1}H-NMR.

ASSOCIATED CONTENT

Supporting Information. Detailed experimental procedures for syntheses and catalysis, characterization data, analytical setups, additional NMR and IR data.

AUTHOR INFORMATION

Corresponding Author

*E-mail: florian.wisser@ircelyon.univ-lyon1.fr

*E-mail: jerome.canivet@ircelyon.univ-lyon1.fr

ORCID

Florian Wisser: 0000-0002-5925-895X

Pierrick Berruyer: 0000-0003-1783-6034

Elsje A. Quadrelli: 0000-0002-8606-1183

Jérôme Canivet: 0000-0002-0458-3085

David Farrusseng: 0000-0002-9093-4143

Author Contributions

The manuscript was written through contributions of all authors. All authors have given approval to the final version of the manuscript.

ACKNOWLEDGMENT

F.M.W. gratefully acknowledges financial support from the Deutsche Forschungsgemeinschaft (DFG, Postdoctoral Research Fellowship, grant number WI 4721/1-1). The authors acknowledge financial support from ERC Advanced Grant No. 320860. The authors are very grateful to N. Cristin and P. Mascunan for ICP-OES analysis, to L. Burel for electron microscopy, to Prof. Dr. G. Kickelbick (Saarland University) for providing access to CHN-analysis and to Dr. O. Ouari and Prof. Dr. P. Tordo (both from Aix-Marseille University) for providing polarizing agent TEKPOL.

REFERENCS

1. Avenier, P.; Taoufik, M.; Lesage, A.; Solans-Monfort, X.; Baudouin, A.; de Mallmann, A.; Veyre, L.; Basset, J. M.; Eisenstein, O.; Emsley, L.; Quadrelli, E. A. *Science* **2007**, *317*, 1056-1060.

2. Copéret, C.; Comas-Vives, A.; Conley, M. P.; Estes, D. P.; Fedorov, A.; Mougel, V.; Nagae, H.; Núñez-Zarur, F.; Zhizhko, P. A. *Chem. Rev.* **2016**, *116*, 323-421.

3. Pelletier, J. D. A.; Basset, J.-M. *Acc. Chem. Res.* **2016**, *49*, 664-677.

4. He, L.-N.; Wang, J.-Q.; Wang, J.-L. *Pure Appl. Chem.* **2009**, *81*, 2069-2080.

5. Rose, M.; Palkovits, R. Catalysis by Covalent Organic Frameworks (COFs). In *Metal Organic Frameworks as Heterogeneous Catalysts*, Llabrés i Xamena, F. X.; Gascon, J., Eds. RSC Catalysis Series nº 12, RSC Publishing: Cambridge, 2013; pp 384-405.

6. Conley, M. P.; Copéret, C. *Top. Catal.* **2014**, *57*, 843-851.

7. Slater, A. G.; Cooper, A. I. *Science* **2015**, *348*.

8. Gunasekar, G. H.; Park, K.; Jung, K.-D.; Yoon, S. *Inorg. Chem. Front.* **2016**, *3*, 882-895.

9. Liu, X.; Inagaki, S.; Gong, J. *Angew. Chem. Int. Ed.* **2016**, *55*, 14924-14950.

10. White, J. L.; Baruch, M. F.; Pander Iii, J. E.; Hu, Y.; Fortmeyer, I. C.; Park, J. E.; Zhang, T.; Liao, K.; Gu, J.; Yan, Y.; Shaw, T. W.; Abelev, E.; Bocarsly, A. B. *Chem. Rev.* **2015**, *115*, 12888-12935.

11. Quadrelli, E. A.; Basset, J.-M. *Coord. Chem. Rev.* **2010**, *254*, 707-728.

12. Wang, L.; Xiao, F.-S. *ChemCatChem* **2014**, *6*, 3048-3052.

13. Pomogailo, A. D.; Wöhrle, D. Synthesis and Structure of Macromolecular Metal Complexes. In *Macromolecule-Metal Complexes*, Ciardelli, F.; Tsuchida, E.; Wöhrle, D., Eds. Springer-Verlag: Berlin Heidelberg, 1996; Vol. 1, pp 11-129.

14. Corma, A.; García, H.; Llabrés i Xamena, F. X. *Chem. Rev.* **2010**, *110*, 4606-4655.

15. Furukawa, H.; Cordova, K. E.; O'Keeffe, M.; Yaghi, O. M. *Science* **2013**, *341*.

16. Cohen, S. M. *Chem. Rev.* **2012**, *112*, 970-1000.

17. Liu, J.; Chen, L.; Cui, H.; Zhang, J.; Zhang, L.; Su, C.-Y. *Chem. Soc. Rev.* **2014**, *43*, 6011-6061.

18. Islamoglu, T.; Goswami, S.; Li, Z.; Howarth, A. J.; Farha, O. K.; Hupp, J. T. *Acc. Chem. Res.* **2017**, *50*, 805-813.

19. McKeown, N. B.; Budd, P. M. *Chem. Soc. Rev.* **2006**, *35*, 675-683.

20. Dawson, R.; Cooper, A. I.; Adams, D. J. *Prog. Polym. Sci.* **2012**, *37*, 530-563.

21. Rogge, S. M. J.; Bavykina, A.; Hajek, J.; Garcia, H.; Olivos-Suarez, A. I.; Sepulveda-Escribano, A.; Vimont, A.; Clet, G.; Bazin, P.; Kapteijn, F.; Daturi, M.; Ramos-Fernandez, E. V.; Llabrés i Xamena, F. X.; Van Speybroeck, V.; Gascon, J. *Chem. Soc. Rev.* **2017**, *46*, 3134-3184.

22. Tan, L.; Tan, B. *Chem. Soc. Rev.* **2017**, *46*, 3322-3356.

23. Dawson, R.; Laybourn, A.; Clowes, R.; Khimyak, Y. Z.; Adams, D. J.; Cooper, A. I. *Macromolecules* **2009**, *42*, 8809-8816.

24. Jiang, J.-X.; Su, F.; Trewin, A.; Wood, C. D.; Campbell, N. L.; Niu, H.; Dickinson, C.; Ganin, A. Y.; Rosseinsky, M. J.; Khimyak, Y. Z.; Cooper, A. I. *Angew. Chem., Int. Ed.* **2007**, *46*, 8574-8578.

25. Xu, Y.; Jin, S.; Xu, H.; Nagai, A.; Jiang, D. *Chem. Soc. Rev.* **2013**, *42*, 8012-8031.

26. Zhou, Y.-B.; Zhan, Z.-P. *Chem. Asian J.*, DOI: 10.1002/asia.201701107.

27. Kaes, C.; Katz, A.; Hosseini, M. W. *Chem. Rev.* **2000**, *100*, 3553-3590.

28. McDaniel, D. H.; Brown, H. C. *J. Org. Chem.* **1958**, *23*, 420-427.

29. Exner, O. The Hammett Equation—the Present Position. In *Advances in Linear Free Energy Relationships*, Chapman, N. B.; Shorter, J., Eds. Springer US: Boston, MA, 1972; pp 1-69.

30. Hansch, C.; Leo, A.; Taft, R. W. *Chem. Rev.* **1991**, *91*, 165-195.

31. Himeda, Y.; Onozawa-Komatsuzaki, N.; Sugihara, H.; Kasuga, K. *Organometallics* **2007**, *26*, 702-712.

32. Cavka, J. H.; Jakobsen, S.; Olsbye, U.; Guillou, N.; Lamberti, C.; Bordiga, S.; Lillerud, K. P. *J. Am. Chem. Soc.* **2008**, *130*, 13850-13851.

33. Bloch, E. D.; Britt, D.; Lee, C.; Doonan, C. J.; Uribe-Romo, F. J.; Furukawa, H.; Long, J. R.; Yaghi, O. M. *J. Am. Chem. Soc.* **2010**, *132*, 14382-14384.

34. Hendon, C. H.; Bonnefoy, J.; Quadrelli, E. A.; Canivet, J.; Chambers, M. B.; Rousse, G.; Walsh, A.; Fontecave, M.; Mellot-Draznieks, C. *Chem. Eur. J.* **2016**, *22*, 3713-3718.

35. Jiang, J.-X.; Su, F.; Trewin, A.; Wood, C. D.; Niu, H.; Jones, J. T. A.; Khimyak, Y. Z.; Cooper, A. I. *J. Am. Chem. Soc.* **2008**, *130*, 7710-7720.

36. Trunk, M.; Herrmann, A.; Bildirir, H.; Yassin, A.; Schmidt, J.; Thomas, A. *Chem. - Eur. J.* **2016**, *22*, 7179-7183.

37. Jiang, J.-X.; Wang, C.; Laybourn, A.; Hasell, T.; Clowes, R.; Khimyak, Y. Z.; Xiao, J.; Higgins, S. J.; Adams, D. J.; Cooper, A. I. *Angew. Chem. Int. Ed.* **2011**, *50*, 1072-1075.

38. Liang, W.; Church, T. L.; Zheng, S.; Zhou, C.; Haynes, B. S.; D'Alessandro, D. M. *Chem. - Eur. J.* **2015**, *21*, 18576-18579.

39. Broicher, C.; Foit, S.; Rose, M.; Hausoul, P. J. C.; Palkovits, R. *ACS Catal.* **2017**, *7*, 8413-8419.

40. Ni, Q. Z.; Daviso, E.; Can, T. V.; Markhasin, E.; Jawla, S. K.; Swager, T. M.; Temkin, R. J.; Herzfeld, J.; Griffin, R. G. *Acc. Chem. Res.* **2013**, *46*, 1933-1941.

41. Rossini, A. J.; Zagdoun, A.; Lelli, M.; Lesage, A.; Copéret, C.; Emsley, L. *Acc. Chem. Res.* **2013**, *46*, 1942-1951.

42. Blanc, F.; Chong, S. Y.; McDonald, T. O.; Adams, D. J.; Pawsey, S.; Caporini, M. A.; Cooper, A. I. *J. Am. Chem. Soc.* **2013**, *135*, 15290-15293.

43. Gascon, J.; Hernández-Alonso, M. D.; Almeida, A. R.; van Klink, G. P. M.; Kapteijn, F.; Mul, G. *ChemSusChem* **2008**, *1*, 981-983.

44. Shen, L.; Liang, R.; Luo, M.; Jing, F.; Wu, L. *Phys. Chem. Chem. Phys.* **2015**, *17*, 117-121.

45. Chaoui, N.; Trunk, M.; Dawson, R.; Schmidt, J.; Thomas, A. *Chem. Soc. Rev.* **2017**, *46*, 3302-3321.

46. Sun, Q.; Dai, Z.; Liu, X.; Sheng, N.; Deng, F.; Meng, X.; Xiao, F.-S. *J. Am. Chem. Soc.* **2015**, *137*, 5204-5209.

47. Wisser, F. M.; Grothe, J.; Kaskel, S. *Sens. Actuators, B* **2016**, *223*, 166-171.

48. Weber, J.; Schmidt, J.; Thomas, A.; Böhlmann, W. *Langmuir* **2010**, *26*, 15650-15656.

49. Boddien, A.; Loges, B.; Junge, H.; Beller, M. *ChemSusChem* **2008**, *1*, 751-758.

50. Fellay, C.; Dyson, P. J.; Laurenczy, G. *Angew. Chem., Int. Ed.* **2008**, *47*, 3966-3968.

51. Himeda, Y. *Green Chem.* **2009**, *11*, 2018-2022.

52. Hull, J. F.; Himeda, Y.; Wang, W.-H.; Hashiguchi, B.; Periana, R.; Szalda, D. J.; Muckerman, J. T.; Fujita, E. *Nat. Chem.* **2012**, *4*, 383-388.

53. Grasemann, M.; Laurenczy, G. *Energy Environ. Sci.* **2012**, *5*, 8171-8181.

54. Yamazaki, Y.; Takeda, H.; Ishitani, O. *J. Photochem. Photobiol., C Photochem. Rev.* **2015**, *25*, 106-137.

55. Liao, W.-M.; Zhang, J.-H.; Hou, Y.-J.; Wang, H.-P.; Pan, M. *Inorg. Chem. Commun.* **2016**, *73*, 80-89.

56. Elgrishi, N.; Chambers, M. B.; Wang, X.; Fontecave, M. *Chem. Soc. Rev.* **2017**, *46*, 761-796.

57. Crake, A. *Mater. Sci. Technol.* **2017**, 1-13.

58. Wang, C.; Xie, Z.; deKrafft, K. E.; Lin, W. *J. Am. Chem. Soc.* **2011**, *133*, 13445-13454.

59. Chambers, M. B.; Wang, X.; Elgrishi, N.; Hendon, C. H.; Walsh, A.; Bonnefoy, J.; Canivet, J.; Quadrelli, E. A.; Farrusseng, D.; Mellot-Draznieks, C.; Fontecave, M. *ChemSusChem* **2015**, *8*, 603-608.

60. Fei, H.; Sampson, M. D.; Lee, Y.; Kubiak, C. P.; Cohen, S. M. *Inorg. Chem.* **2015**, *54*, 6821-6828.

61. Lee, Y.; Kim, S.; Fei, H.; Kang, J. K.; Cohen, S. M. *Chem. Commun.* **2015**, *51*, 16549-16552.

62. Sun, D.; Gao, Y.; Fu, J.; Zeng, X.; Chen, Z.; Li, Z. *Chem. Commun.* **2015**, *51*, 2645-2648.

63. Kajiwara, T.; Fujii, M.; Tsujimoto, M.; Kobayashi, K.; Higuchi, M.; Tanaka, K.; Kitagawa, S. *Angew. Chem., Int. Ed.* **2016**, *55*, 2697-2700.

64. Wang, C.; Xie, Z.; deKrafft, K. E.; Lin, W. *ACS Appl. Mater. Interfaces* **2012**, *4*, 2288-2294.

65. Wang, J.-L.; Wang, C.; deKrafft, K. E.; Lin, W. *ACS Catal.* **2012**, *2*, 417-424.

66. Haikal, R. R.; Wang, X.; Hassan, Y. S.; Parida, M. R.; Murali, B.; Mohammed, O. F.; Pellechia, P. J.; Fontecave, M.; Alkordi, M. H. *ACS Appl. Mater. Interfaces* **2016**, *8*, 19994-20002.

67. Wang, C.-A.; Han, Y.-F.; Li, Y.-W.; Nie, K.; Cheng, X.-L.; Zhang, J.-P. *RSC Adv.* **2016**, *6*, 34866-34871.

68. Zhou, Y.-B.; Wang, Y.-Q.; Ning, L.-C.; Ding, Z.-C.; Wang, W.-L.; Ding, C.-K.; Li, R.-H.; Chen, J.-J.; Lu, X.; Ding, Y.-J.; Zhan, Z.-P. *J. Am. Chem. Soc.* **2017**, *139*, 3966–3969.

69. Pullen, S.; Ott, S. *Top. Catal.* **2016**, 1-10.

70. Hawecker, J.; Lehn, J.-M.; Ziessel, R. *J. Chem. Soc., Chem. Commun.* **1985**, 56-58.

71. Lehn, J.-M.; Ziessel, R. *J. Organomet. Chem.* **1990**, *382*, 157-173.

72. Canivet, J.; Bonnefoy, J.; Daniel, C.; Legrand, A.; Coasne, B.; Farrusseng, D. *New J. Chem.* **2014**, *38*, 3102-3111.

73. Vermoortele, F.; Vandichel, M.; Van de Voorde, B.; Ameloot, R.; Waroquier, M.; Van Speybroeck, V.; De Vos, D. E. *Angew. Chem. Int. Ed.* **2012**, *51*, 4887-4890.

74. Vandichel, M.; Hajek, J.; Vermoortele, F.; Waroquier, M.; De Vos, D. E.; Van Speybroeck, V. *CrystEngComm* **2015**, *17*, 395-406.

75. Alkorta, I.; Elguero, J.; Roussel, C.; Vanthuyne, N.; Piras, P. Atropisomerism and axial chirality in heteroaromatic compounds. In *Advances in Heterocyclic Chemistry*, Katritzky, A., Ed. Academic Press: 2012; pp 1-188.

76. Pulukkody, R.; Kyran, S. J.; Drummond, M. J.; Hsieh, C.-H.; Darensbourg, D. J.; Darensbourg, M. Y. *Chem. Sci.* **2014**, *5*, 3795-3802.

77. Kelly, J. M.; M. O'Connell, C.; Vos, J. G. *Inorg. Chim. Acta* **1982**, *64*, L75-L76.

78. Smieja, J. M.; Kubiak, C. P. *Inorg. Chem.* **2010**, *49*, 9283-9289.

79. Himeda, Y.; Miyazawa, S.; Hirose, T. *ChemSusChem* **2011**, *4*, 487-493.

80. Dinda, S.; Patwardhan, A. V.; Pradhan, N. C. *Ind. Eng. Chem. Res.* **2006**, *45*, 6632-6639.

81. Flaig, R. W.; Osborn Popp, T. M.; Fracaroli, A. M.; Kapustin, E. A.; Kalmutzki, M. J.; Altamimi, R. M.; Fathieh, F.; Reimer, J. A.; Yaghi, O. M. *J. Am. Chem. Soc.* **2017**, *139*, 12125–12128.

Table of Contents

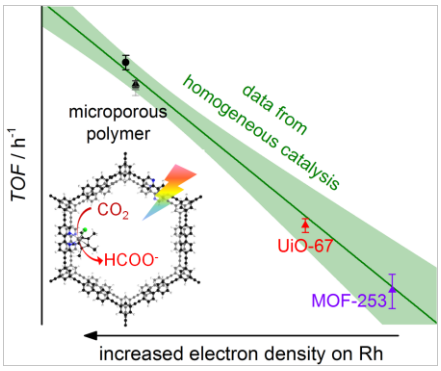
TOF / h-1
microporous
polymer
CO2
HCOO-
data from
homogeneous catalysis
UiO-67
MOF-253
increased electron density on Rh